CHEMISTRY OF MATERIALS

Article

pubs.acs.org/cm

Thermoreversible Reactions on Inorganic Nanoparticle Surfaces: Diels–Alder Reactions on Sterically Crowded Surfaces

Tom Engel and Guido Kickelbick*

Inorganic Solid State Chemistry, Saarland University, Am Markt Zeile 3, 66125 Saarbrücken, Germany

Supporting Information

ABSTRACT: Organically surface-functionalized nanoparticles are important cross-linkers for nanocomposites. In the past, many cross-linking reactions were based on simple radical additions. However, novel smart materials require reversible reactions. These reactions, such as the Diels–Alder reaction, often have a specific sterical demand, e.g., a six-centered transition state. In this study, < 5 nm silica particles were functionalized with maleimide groups, and their reactivity with regard to Diels–Alder reactions were investigated, applying various techniques. A new method for the surface modification of silica nanoparticles is presented, minimizing agglomeration in organic solvents and thus increasing the accessibility of the functional groups on the particle surface. Kinetic studies of substituted model compounds were carried out to evaluate the reactivity of the maleimide functionality. The Diels–Alder reaction between 2,5-dimethylfuran and *N*-propylmaleimide, *N*-ethyl(*N*-propylcarbamato)maleimide, and *N*-phenylmaleimide was followed by UV/Vis spectroscopy. The reaction rate increases in this order, showing the effect of maleimide substitution. Afterwards *N*-((3-triethoxysilyl)propyl)maleimide was used to graft maleimidopropyl functional groups onto the nanoparticle surface. 3-Aminopropyltriethoxysilane, which could then be reacted with 1,1′-(methylenedi-4,1-phenylene)bismaleimide, was used to attach phenyl-substituted maleimide functionality to the surface. 3-Isocyanatopropyltriethoxysilane introduced the electron-drawing carbamato functionality into the system. The surface coverage of the samples was characterized applying CHN analysis, TGA-FTIR coupling, and FTIR spectroscopy. All analytical methods revealed that the functional groups are covalently bonded to the silica surface and the maleimide rings remain intact. Diels–Alder reactions of the surface groups show that the reactivity of the molecules attached to the particles depends on sterical crowding, but the reaction rate is not significantly changed by surface effects.

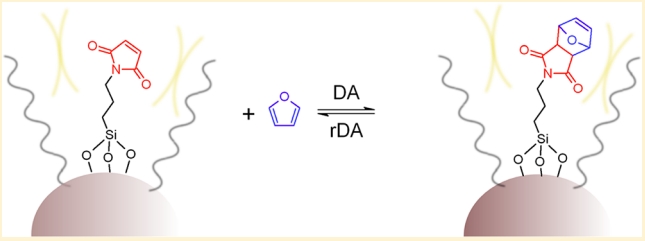

KEYWORDS: *nanoparticles, surface-functionalization, thermoreversible reaction, Diels–Alder*

INTRODUCTION

Inorganic nanoparticles are important building blocks for many novel materials. The incorporation of nanoparticles in polymer matrixes can dramatically change their properties. Particularly the mechanical and thermal properties are influenced by the incorporated inorganic phase. In many cases it is necessary to provide a surface-functionalization to enhance the compatibility and the dispersion of the nanoparticles in an organic matrix.[1,2] Changing the polarity and the availability of functional groups has a significant effect on the dispersibility in the monomer or polymer matrix and allows a tight bonding to the latter by the formation of cross-linked networks. The grafting of polymerizable functional groups onto the nanoparticle surface allows covalent bonding with the matrix, improving the compatibility of the phases and preventing phase separation and agglomeration of particles.[2,3] Methacryloxy and epoxy functionalities have been used to incorporate silica nanoparticles into organic matrixes through copolymerization.[3] This increases homogeneity of the particle distribution and also mechanical strength of the resulting nanocomposite. A drawback of highly cross-linked materials is crack formation and crack propagation. In addition, the often observed absence of glass transition and melting points prevents the cross-linked nanocomposite from being reprocessed and reshaped.

In recent years, compounds with reversible bonding became the focus of materials scientists, due to self-healing properties and the possibility to reprocess and reshape cross-linked nanocomposites.[4−8] One of the major mechanisms used in this respect is the Diels–Alder (DA) reaction, applying maleimide and furan functional groups as dienophiles and dienes. Due to the thermoreversible reaction type these materials show also a self-healing ability.

Wudl et al. were the first to synthesize a thermally remendable macromolecule and to investigate its self-healing properties.[4] They found that cuts or cracks could be healed by a simple thermal treatment. Our aim is the combination of reversible DA chemistry with the advantages of nanocomposite materials.

By using reversible DA cross-linking, the inorganic particles can be separated from the polymer matrix by a simple thermal

Received: September 21, 2012
Revised: December 7, 2012

   dx.doi.org/10.1021/cm303049k | *Chem. Mater.* XXXX, XXX, XXX–XXX

treatment. Beyer et al. used reversible DA chemistry to develop polymer films in which a change in optical clarity can be thermally triggered.[9] Rahman et al. grafted free maleimide functional groups through nucleophilic addition of a commercially available bismaleimide onto the surface of amino-functionalized silica nanoparticles.[10] They investigated the reactivity of the maleimide groups to undergo Michael reaction on the surface of the particles.

In the same spirit we investigated the surface functionalization of silica nanoparticles with maleimide functional groups. An important aspect of our work was the investigation of the reactivity of the dienophiles on the surface of nanoparticles. Because of the sterical hindrance and the demand of a six-membered transition state for the DA reaction, it is important to judge the effect of sterical crowded surfaces on this reaction type. Therefore, different coupling agents with maleimide functionality were synthesized and grafted onto particles, and the surface coverage was determined. A model reaction with furan was used to investigate the influence of steric hindrance on DA and retro-Diels–Alder (retro-DA) chemistry.

RESULTS AND DISCUSSION

Synthesis and Characterization of Silica Nanoparticles. Spherical amorphous silica nanoparticles were prepared following a modified Stöber process.[11] Tetraethyl orthosilicate (TEOS) was first hydrolyzed and then condensed in alcoholic solution, applying ammonia as base. Transmission electron microscopy (TEM) (Figures S1 and S2, Supporting Information) and dynamic light scattering (DLS) measurements of the obtained nanoparticles in methanol revealed a diameter of 3.8 ± 0.9 nm and 4.8 ± 0.8 nm, respectively. Nitrogen sorption measurements were performed to calculate the surface area of particles according to Brunauer, Emmett, and Teller (BET).[12] The nitrogen sorption measurement shows a specific surface area of 750 m^2 per gram of silica nanoparticles. When assuming a spherical shape of the particles and a density for silica of 2.2 g cm^{-3}, the calculated diameter is 3.6 nm, which corresponds to the diameter measured in the TEM experiment. Some discrepancy may be explained by porosity. The physisorption isotherm revealed a characteristic hysteresis loop, which is associated with capillary condensation taking place in mesopores (IUPAC Type IV H2).[13]

Surface functionalization was carried out by applying a solvent-exchange methodology, which allows for higher surface coverage and very low agglomeration of the particles.[14] Isobutyl methyl ketone (IBMK) was used as the suspension medium for the silica particles during the modification step because of its relatively high dielectric constant, ε = 13.1, which results in ionized hydroxyl groups on the nanoparticle surface. Another advantage of this solvent is the relatively high boiling point of 115 °C, which favors the elimination of ethoxy groups and condensation of the silane coupling agents during functionalization reactions.

In previous studies, toluene was the preferred solvent because of the high boiling point, but its low dielectric constant of ε = 2.4 made it a poor choice because the particle suspension is not stable in toluene and the particles tend to agglomerate. Green et al. isolated the bare silica particles and redispersed them in IBMK after drying.[14] In this work, it was examined if the solvent could be changed without isolation of the particles. Therefore, IBMK was added to a freshly prepared silica suspension in methanol, and the two solvents were codistilled by rotary evaporation. This step was repeated two times. Dynamic light scattering measurements before and after the solvent exchange showed that the particle suspensions remained stable during this procedure (Figure 1).

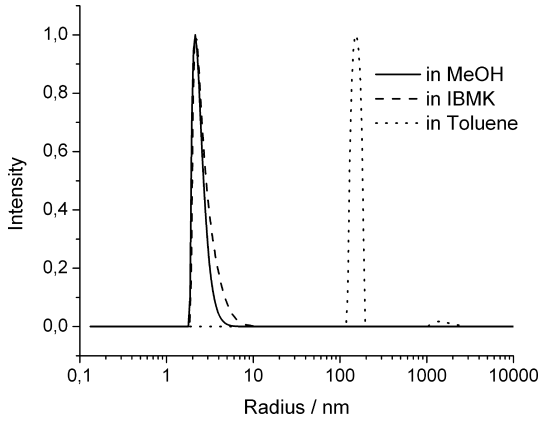

Figure 1. DLS size distribution of silica particles before and after solvent exchange and after suspension in toluene.

The particles in the original alcoholic dispersion had a diameter of 4.8 ± 0.8 nm. The particles transferred to IBMK showed a diameter of 5.4 ± 1.2 nm (DLS). In addition, Figure 1 shows the size distribution plot of the same silica particles if suspended in toluene. Agglomerates with a diameter of more than 300 nm were formed in toluene.

Coupling Agents. Different coupling agents for the surface modification of the nanoparticles were used. *N*-((3-Triethoxysilyl)propyl)maleimide **1**, 2-(2,5-dioxo-2,5-dihydro-1*H*-pyrrol-1-yl)ethyl(3-(triethoxysilyl)propyl)carbamate **2**, and 1-(4-{[4-(2,5-dioxo-3-{[3-(triethoxysilyl)-propyl]amino}-pyrrolidin-1-yl)phenyl]methyl}phenyl)-2,5-dihydro-1*H*-pyrrole-2,5-dione **3**. These molecules are composed of a triethoxysilane anchor group, a spacer, and a maleimide functional group used as the dienophile functionality for DA reaction.

1 was synthesized according to a literature procedure (Scheme 1)[15] with an overall yield of 96%.

Scheme 1. Reaction Scheme for the Preparation of 1[a]

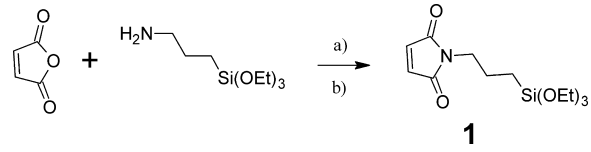

1

[a]Reagents and conditions: (a) dry DCM, RT, 1 h; (b) ZnCl, HMDS, dry toluene, 80 °C, 5 h.

2 was prepared according to a modified literature procedure via a dibutyltin dilaurate-catalyzed addition of protected 2-hydroxyethylmaleimide with *N*-(3-isocyanoato-propyl)-triethoxysilane (Scheme 2).[16] The protection of maleimide functionality with furan via DA reaction is necessary because 2-hydroxyethylmaleimide tends to polymerize via Michael addition of the hydroxyl group to the maleimide double bond. Deprotection takes place during the surface modification step of the silica nanoparticles. The boiling point of the suspension medium IBMK is sufficiently high to provoke retro-DA reaction with liberation of furan.

dx.doi.org/10.1021/cm303049k | *Chem. Mater.* XXXX, XXX, XXX–XXX

Scheme 2. Reaction Scheme for the Preparation of 2[a]

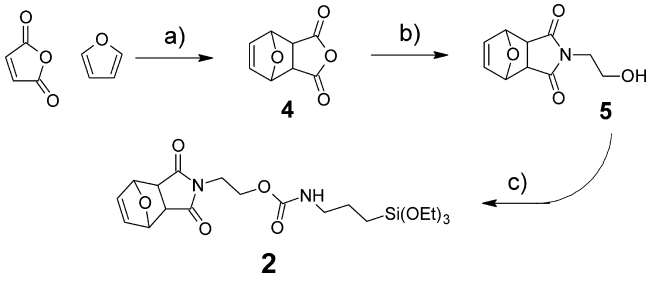

[a]Reagents and conditions: (a) Toluene, rt, 24 h; (b) ethanolamine, dry MeOH, reflux, 24 h; (c) isocyanatopropyltriethoxysilane, dibutyltin dilaurate, acetone, reflux, 12 h.

Commercially available APTES was used to react with 1,1′-(methylendi-4,1-phenylene)bismaleimide via Michael addition as shown in Scheme 3 to form **3**.

Surface Modification and Characterization. Dynamic Light Scattering. DLS was used to investigate the dispersibility of the isolated particles, which is an important proof of the availability of the functional groups at the surface. The particles were mixed with different solvents, and they were sonicated for 10 min. For **1**@SiO_2 and **2**@SiO_2, the best results were achieved with 2-propanol as suspension medium (Figure 2). The other solvents resulted in agglomerates of more than 100 nm. Only suspension in 2-propanol resulted in a narrow distribution around 15 and 60 nm, respectively. This could be explained by the duality of the 2-propanol properties. On the one hand, it has a hydroxyl group, which can undergo hydrogen bonding with either the particle surface or the carbonyl groups of the maleimide ring, and on the other hand, it has an isopropyl chain, which can develop weak interactions with the surface functionalities. **3**@SiO_2 was not dispersible in 2-propanol and most other suspension mediums. The best result, a relatively broad size distribution of 100 nm, was achieved in dimethylformamide (DMF). This study shows how critical the suspension medium is for the accessibility of the functional groups.

FTIR Analysis. The success of functionalization was studied by FTIR spectroscopy (Figure 3). All samples showed multiple peaks in the "fingerprint"-region of silica between 460 and 1200 cm^{-1}: A strong asymmetric Si−O−Si vibration at about 1100 cm^{-1}, weaker asymmetric Si−OH vibration at 957 cm^{-1}, symmetric Si−O−Si vibration at 797 cm^{-1}, and two additional peaks at 573 and 460 cm^{-1}.[17] The FTIR spectrum of pure silica shows the presence of molecular water through scissor bending vibration at ∼1630 cm^{-1}. The broad signal between 3300 and 3700 cm^{-1} is a superimposition of H-bonded molecular water and hydroxyl terminals of silanol groups. An O−H stretching vibration, characteristic of free surface silanol groups, was only detected in the pure silica sample at 3746 cm^{-1}.[18] CH_2 and CH_3 (2907, 2945, and 2984 cm^{-1}) vibrational modes can be assigned to the remaining ethoxy groups on the surface of the

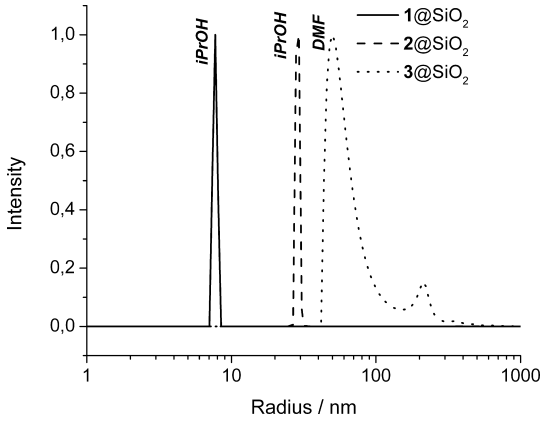

Figure 2. Dynamic light scattering size distributions of **1**@SiO_2 in 2-propanol, **2**@SiO_2 in 2-propanol, and **3**@SiO_2 in DMF.

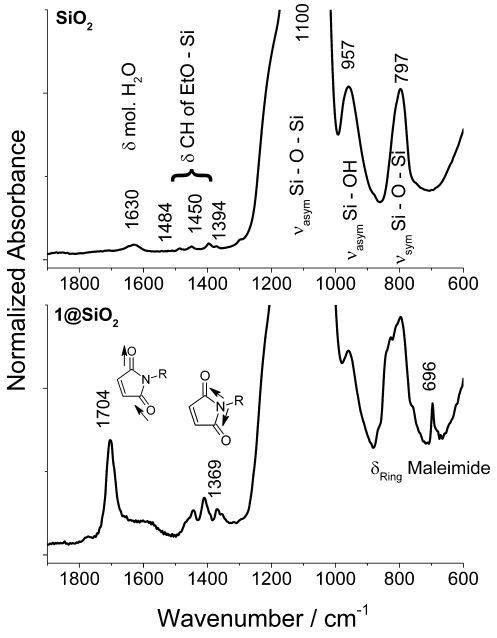

Figure 3. Infrared spectra of bare silica and the sample modified with **1**.

Scheme 3. Reaction Scheme for the Preparation of BMPTES

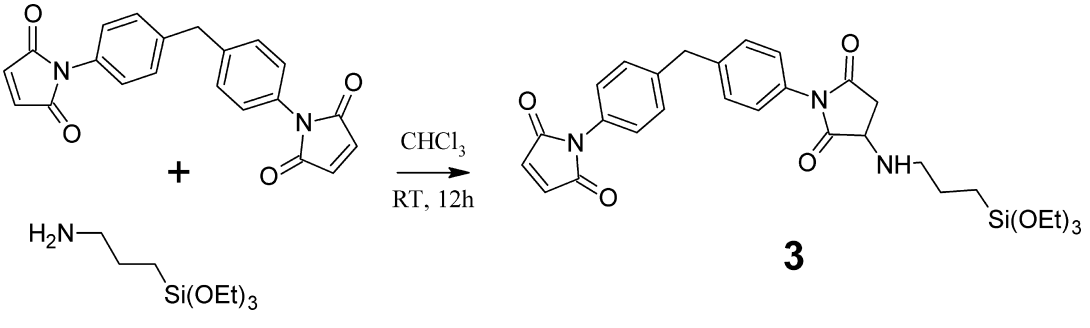

dx.doi.org/10.1021/cm303049k | Chem. Mater. XXXX, XXX, XXX−XXX

nanoparticles as well as the weak signals at 1484, 1450, and 1394 cm^{-1}, which rise from C−H bending modes..

Attenuated total reflection infrared (ATR-FTIR) measurements of the **1**-functionalized particles revealed characteristic signals for organic coupling agents (Figure 3). The strong asymmetric stretch of the carbonyls could be detected at 1704 cm^{-1}, and even the weak symmetric stretching mode is visible at 1770 cm^{-1}. The symmetric C−N−C stretching vibration at 1369 cm^{-1} is another proof of the successful functionalization with maleimide functionality. Another indication for the high surface modification is the peak at 696 cm^{-1} assigned to maleimide ring deformation.[19]

The FTIR spectrum of **3**@SiO_2 (Figure S4, Supporting Information) shows signals for both the symmetric and asymmetric stretching modes of the conjugated maleimide carbonyl groups at 1773 cm^{-1} (very weak) and 1714 cm^{-1} (strong). The last mentioned signal is stronger than all the other carbonyl signals because the surface molecules are composed of two imides. The signal at 1513 cm^{-1} could be assigned to aromatic C−C stretching mode of the benzene rings and the peak at 1388 cm^{-1} is caused by a symmetric C−N−C stretching vibration within the maleimide ring as shown by Parker et al.[19]

In the spectrum of **2**@SiO_2 (Figure S3, Supporting Information), both symmetric and asymmetric stretching modes of carbonyls at 1773 cm^{-1} and 1710 cm^{-1} were present but the signals are weaker because of lower surface coverage. Weak C−H bending modes could be observed at 1439 cm^{-1} and 1409 cm^{-1}. A signal at 1546 cm^{-1} could arise from maleimide C═C stretching or N−H bending of the urethyl group. The high amount of surface modification is also verified by the maleimide ring deformation at 697 cm^{-1}.

Thermogravimetric Analysis. TGA was coupled with infrared spectroscopy to investigate the thermal stability of modified particles. The three-dimensional IR plots are shown in Figures S5−S7, Supporting Information. The temperature-dependent mass loss of **1**@SiO_2 revealed two discernible steps. The first one at 110−300 °C released mainly IBMK adsorbed to the particle surface and ethanol from excess ethoxy groups not reacted during condensation. This mass loss totaled 6%. The second step from 300 °C to 700 °C released CO_2, ammonia, water, carbon monoxide, and ethylene, pointing to the thermal decomposition of the maleimidopropyl functionality. During this step 17.5% of the initial mass was lost. Burning of residual carbon under oxygen released additional 6.5%. According to the TGA measurements, 24% of the mass of the **1**@SiO_2 sample could be assigned to the coupling agent.

The temperature-dependent mass loss of **3**@SiO_2 showed three discernible steps. The first one at 30−200 °C released water adsorbed to the particle surface and ethanol from excess ethoxy groups not reacted during condensation. This mass loss totaled 1.2%. The second step from 200 °C to 360 °C released CO_2, ammonia, water, carbon monoxide, and an organic acid, pointing to the thermal decomposition of the maleimido-functionality. During this step 3.2% of the initial mass was lost. The third decomposition step released 22.4% of CO_2, water, CO and ethylene. Burning of residual carbon under oxygen released additional 13.7%. According to the TGA measurements, about 39% of the mass of the **3**@SiO_2 sample could be assigned to the coupling agent.

The temperature dependent mass loss of **2**@SiO_2 showed three discernible steps. The first one at 30−150 °C released water adsorbed to the particle surface and ethanol from excess ethoxy groups not reacted during condensation. This mass loss totaled 2.0%. The second step from 150 °C to 310 °C released CO_2, ammonia, water, carbon monoxide, and an organic acid, pointing to the thermal decomposition of the maleimido functionality. During this step, 3.3% of the initial mass was lost. The third decomposition step released 14.0% of CO_2, water, CO, and ethylene. No residual carbon was burned under oxygen. According to the TGA measurements, about 17% of the mass of the **2**@SiO_2 sample could be assigned to the coupling agent.

Elemental Analysis. The percentage of nitrogen is the perfect tool to calculate the number of functional groups on the surface of the silica particles, because the nitrogen atoms are only present in the coupling agent and not in residual solvent or ethoxy groups. Equation 1 gives the molar amount of functional groups per gram of particles. This calculation gave 1.5 ± 0.2, 0.3 ± 0.1, and 1.3 ± 0.1 mmol of maleimide per gram of particle for **1**@SiO_2, **2**@SiO_2, and **3**@SiO_2, respectively.

By taking into account the surface area per gram of silica, the number of functional groups per surface area could be calculated (eq 2) and resulted in the following surface coverages: 1.2 ± 0.2 functional groups per nm^2 for **1**@SiO_2; 0.3 ± 0.1 functional groups per nm^2 for **2**@SiO_2; 1.0 ± 0.1 functional groups per nm^2 for **3**@SiO_2.

Diels−Alder Reaction on the Surface of Nanoparticles. The particles were reacted with furan at room temperature to prove their ability to carry out DA reactions. All three samples were isolated and were dispersed in furan by sonication. The suspensions were stirred for 2 days at RT. Afterward the particles were collected by centrifugation, washed three times with diethyl ether, and dried in vacuum. ATR-FTIR, TGA-IR, and elemental analysis were used to characterize the samples F-**1**@SiO_2, F-**2**@SiO_2, and F-**3**@SiO_2.

Afterward retro-DA reaction was carried out at 150 °C in a vacuum-oven. TGA measurements were used to determine the difference in mass loss between the samples before and after retro-DA reaction.

Figure 4 shows a comparison between the IR spectra of **1**@SiO_2 and F-**1**@SiO_2. The first difference is the small red-shift of

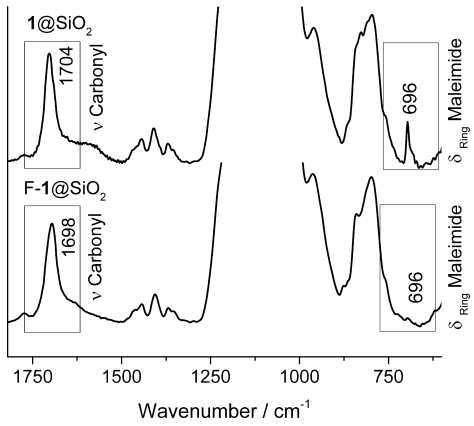

Figure 4. Comparison of **1**@SiO_2 and F-**1**@SiO_2 by infrared spectroscopy.

the carbonyl peak from 1704 to 1698 cm^{-1}, which could be explained by breaking the conjugation between the carbonyls and the maleimide double bond during DA reaction. On the other hand, the maleimide ring deformation signal at 696 cm^{-1} disappeared almost completely. The integration of this signal

dx.doi.org/10.1021/cm303049k | *Chem. Mater.* XXXX, XXX, XXX−XXX

was used to follow the conversion over time of the maleimide system to the DA product.

F-**2**@SiO_2 showed the same vibrational changes, but the changes were more difficult to observe. The red-shift of the carbonyl peak is partly overlapped by the signal of the carbamate. Furthermore, the maleimide ring deformation disappeared during the reaction, but initially the signal was very weak.

No clear differences in the spectra of F-**3**@SiO_2 and **3**@SiO_2 could be observed. The red-shift is covered by carbonyl stretching modes of the additional imide and several signals in the region between 700 and 650 cm^{-1} overlap with the deformation of the maleimide ring, making it impossible to distinguish between these signals.

A comparison of the thermal decomposition between **1**@SiO_2 and F-**1**@SiO_2 showed a larger mass loss in the sample reacted with furan (Figure 5). The difference between the two

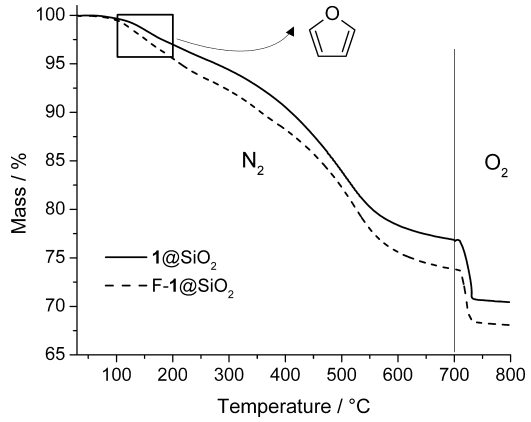

Figure 5. Comparison of TGA measurements of **1**@SiO_2 and F-**1**@SiO_2.

samples represented 1.62%. This difference was determined from 100 °C to 200 °C because IR measurements of the decomposition gases showed that furan is liberated in between these temperatures. Furan, released by retro-DA reaction, was detected by IR spectroscopy showing the typical strong signal at 745 cm^{-1} characteristic for furan (Figure 6). The maximum release of furan from the sample was detected at 135 °C. Above this temperature, ideal reaction conditions for the rDA reaction

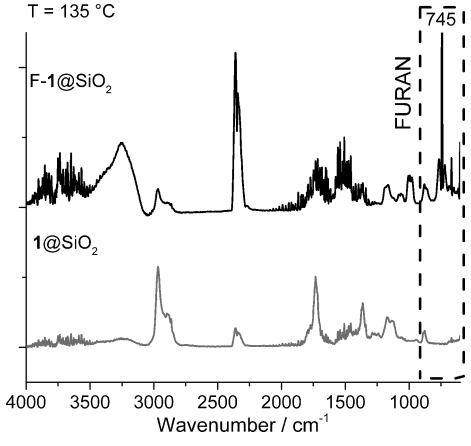

Figure 6. IR Spectra of the decomposition gases at 135 °C of samples **1**@SiO_2 and F-**1**@SiO_2.

on the surface of nanoparticles should be fulfilled. This 1.62% equals 0.24 mmol furan per gram of particles reacted via DA reaction to the maleimide surface groups. Comparing this value with the number of functional groups per gram of particles, the percentage of groups reacting with furan equals 16%.

TGA of F-**2**@SiO_2 gave rise to an additional mass loss of 0.75% between 100 °C and 200 °C (Figure S8, Supporting Information). Taking into account the number of functional groups on the surface of the particles, we could estimate a conversion of 37% of the **2** moieties. F-**3**@SiO_2 liberates 1.50% furan, meaning that 17% of the maleimde groups reacted with furan (Figure S9, Supporting Information).

These results suggest that the percentage of maleimide moieties reacting with furan depends on the surface coverage of the particles and not on the type of surface modification. The more the surface of the particles is crowded, the less of the functional groups are able to react. In total, **1**@SiO_2 shows the highest amount of furan reacted via DA reaction because these samples show the highest surface coverage of 1.2 molecules per nm^2, but relative to surface coverage it exhibited the lowest reactivity. **2**@SiO_2, which presented a much lower coverage of 0.3 molecules per nm^2, showed higher reactivity with respect to the number of functional groups. **1**@SiO_2 expressed four times as many maleimides on the surface than **2**@SiO_2 but only twice as much furan reacted via DA reaction. This observation suggests that there is an ideal number of surface molecules per nm^2 where both effects are compensated.

Elemental analysis results could not be analyzed as easily because the different decomposition steps cannot be distinguished and only carbon, hydrogen, and nitrogen composition can be obtained. The nitrogen content followed the same trend as the TGA results. For all three samples, the relative nitrogen content was lower if the samples were reacted with furan.

Kinetic Studies of Differently Funtionalized Maleimides. The DA reaction between maleimides with various pendant groups and dimethylfuran (MF) was studied with UV spectroscopy and compared to the surface-functionalized nanoparticles. All the reactions followed the same scheme as that shown in Scheme 4.

Scheme 4. General Reaction Scheme for Model DA Reactions

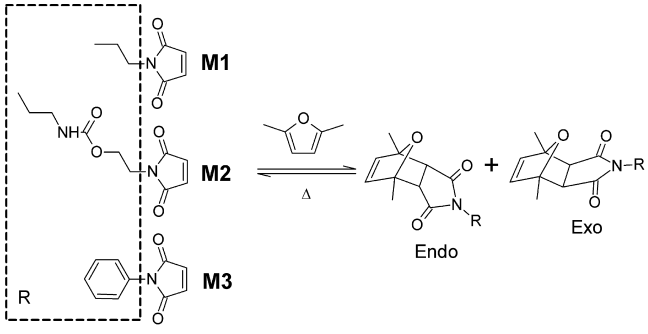

The proportions of exo and endo products are not relevant in the context of the use of DA reaction as a cross-linking reaction between nanoparticles and macromolecular systems. Kinetic studies were only performed to compare reactivity of the maleimdes and to study the effects of different functionalities on the rate constant *k*. Given the structures of the used coupling agents for particle functionalization, we chose three different model compounds for preliminary kinetic

dx.doi.org/10.1021/cm303049k | *Chem. Mater.* XXXX, XXX, XXX–XXX

studies. These model compounds were *N*-propylmaleimide **M1**, *N*-ethyl(*N*-propylcarbamato)maleimide **M2**, and *N*-phenylmaleimide **M3**, respectively. Whereas the UV spectrum of MF in 1,2-dichloroethane did not show any absorption above 270 nm, **M1** in the same solvent (c = 0.02 M) displayed a characteristic maximum at about 290 nm (ε_λ = 656 M^{-1} cm^{-1}) arising from the excitation of the conjugated system of C═C and C═O bonds. During the reaction and as the DA products form, this conjugation breaks, which results in the hipsocromic shift of the absorption corresponding now to the excitation of the remaining carbonyls. The progress of DA reaction could therefore be followed by UV spectroscopy by keeping track of the decrease of the absorbance at 290 nm (for **M1**) with time. This was carried out for the three molecules at different temperatures, specifically 50 °C, 60 °C, and 70 °C. The maximum absorptions for **M2** and **M3** were at 298 nm (ε_λ = 348 M^{-1} cm^{-1}) and 295 nm (ε_λ = 457 M^{-1} cm^{-1}), respectively. Figures S10−S12 (Supporting Information) show the results of kinetic measurements of the three molecules at 60 °C with a 30-fold excess of MF. The high excess of MF was chosen to guarantee pseudo-first-order kinetics with regard to the maleimides and to minimize reaction time. A first experiment with a 10-fold excess of MF lasted several hours, so the concentration of MF was tripled.

Figure S10 shows the natural logarithm of the conversion over time of the three different model maleimides. Table 1 lists

Table 1. Reaction Rate Constants k for Temperatures 50 °C, 60 °C, and 70 °C for Model DA Reactions (confidence interval 95%)

model compound	k [10^{-4} s^{-1}], T = 50 °C	k [10^{-4} s^{-1}], T = 60 °C	k [10^{-4} s^{-1}], T = 70 °C
M1	3.8 ± 0.1	6.2 ± 0.1	12.0 ± 0.3
M2	9.0 ± 0.6	13.3 ± 1.0	15.8 ± 2.7
M3	11.9 ± 0.6	21.6 ± 1.7	28.8 ± 0.4

the reaction rate constants k for each temperature as calculated from the slope of the graphics in Figures S13−15, Supporting Information. Only the linear domain was used to calculate the rate constants because the reactions are not quantitative. The back reaction takes place in different amounts depending on the temperature and the nature of maleimides. As we were only interested in a comparison of the rate at which the reactions take place, we do not take into account measurements near the reaction equilibrium.

Analysis at the k values at 50 °C showed that **M1** is the slowest reactant for the conversion with MF because the propyl chain increases the electron density in the maleimide system, raising the energy level of the LUMO of the dienophile and therefore decreasing energy compatibility of reactive orbitals. The urethyl functionality in **M2** is withdrawing electron density from the maleimide system, therefore lowering the energy level of the LUMO and increasing the interaction with the HOMO of the diene. The phenyl ring of **M3** withdraws even more electron density from the system, which results in even a higher reaction rate constant with regard to **M1**.

Kinetic Studies at the Surface of Particles with Furan at RT. To investigate if the reaction rate is drastically changed at the surface of nanoparticles, the reaction rate constant was estimated by monitoring the maleimide ring deformation signal in the infrared spectra during DA reaction on the surface of silica nanoparticles. Unfortunately, this method could only be used for the propylmaleimide **1**-modified samples because integration of the signal at 696 cm^{-1} over time gave no evaluable results for the other samples. A 200 mg amount of **1**@SiO_2 was dispersed in 20 mL of 2-propanol, and 1 mL of furan was added. Samples were withdrawn from this suspension after various time intervals. The samples were dried immediately, and ATR-IR measurements were carried out (Figure 7). The spectra were normalized using the strongest

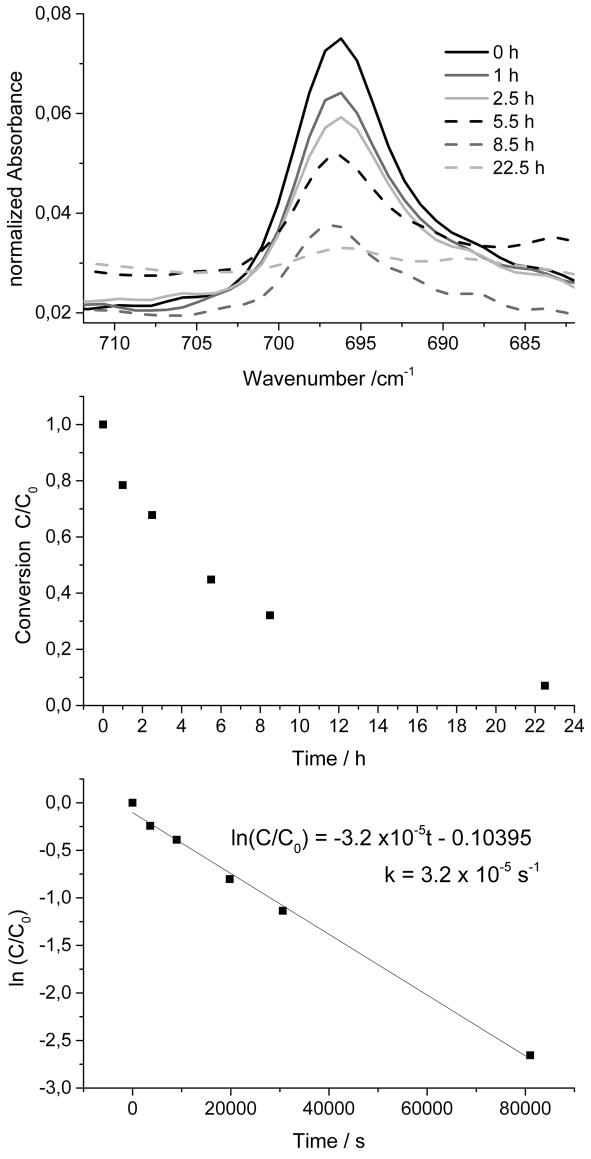

Figure 7. (a) Infrared spectra of **1**@SiO_2 at different time intervals during the reaction with furan. (b) Conversion over time plot. (c) Plot for first-order kinetics as a function of the linear fit and reaction rate value k.

unchanged signal, the asymmetric Si−O−Si stretching, as reference to obtain quantitative information. After a basis line correction, the area under the signal at 696 cm^{-1} was used to plot the conversion against reaction time. The conversion follows exponential decay, as in the case for first-order kinetics (Figure 7). The kinetic rate constant is in the order of 10^{-5} s^{-1}. This value is in the same order of magnitude as that for the reaction rate in the case of molecular systems at room temperature, meaning that the reaction rate is not significantly

dx.doi.org/10.1021/cm303049k | *Chem. Mater.* XXXX, XXX, XXX−XXX

altered by surface effects. UV/Vis spectroscopic measurements could not be performed because of the light scattering properties of the silica nanoparticles.

CONCLUSIONS

This study ascertained that the conditions chosen to conduct surface modification of nanosized silica particles, involving an exchange of the suspension medium from methanol to IBMK, ensures high surface coverage and low agglomeration of the particles. The low dielectric constant of toluene makes it a poor choice because ionization of surface silanols is unlikely.

Another goal of this work was to determine the reactivity of differently substituted maleimides. It was shown in molecular systems that phenyl-substituted maleimides are three times more reactive than propyl-substituted maleimdes. Furthermore, it has been demonstrated that the amount of active sites for the DA reaction on the surface of silica nanoparticles is dependent on the grafting density of the dienophile species. The higher the grafting density and the sterical effects near the reaction site, the lower the conversion of DA reaction. Already reacted furan/maleimide groups interfere with other approaching furan molecules, hindering the continuation of DA reaction. Finally, a kinetic study of DA reactions between maleimide moieties on surfaces and molecular furan has shown that surface effects do not dramatically decrease the reaction rate.

EXPERIMENTAL SECTION

Methods. Fourier transform infrared spectroscopy (FT-IR) measurements were performed on a Bruker Vertex 70 Spectrometer under ambient air (40 scans at a resolution of 4 cm^{-1}) in attenuated total reflectance (ATR) mode. Thermogravimetric analysis (TGA) were performed on a Netzsch Iris TG 209 C in an alumina crucible heating from room temperature to 700 °C under nitrogen followed by heating to 800 °C under oxygen with a rate of 20 K min^{-1}. Differential scanning calorimetry (DSC) measurements were carried out on a Netzsch DSC 204 F1 Phoenix calorimeter in aluminum crucibles with pierced lids, heating under nitrogen with a rate of 15 K min^{-1}. Liquid-state NMR spectra were recorded on a Bruker AC 200F spectrometer (^1H at 200.13 MHz, ^{13}C at 50.32 MHz). Liquid-state ^{29}Si NMR spectra were recorded on a Bruker Avance 300 spectrometer at 69.63 MHz. Elemental analysis was carried out on a Leco 900 CHN Analysator. The percentage of nitrogen was used to calculate the number of functional groups on the surface of the silica particles. Equation 1 gives the molar amount of functional groups per gram of particles:

$$c_{FG} = \frac{100}{\Delta m_{SiO_2}} \times \frac{\Delta m_N}{M_N} \times \frac{0.01}{N} \quad (1)$$

where c_{FG} is the molar concentration of functional groups per gram [mol g^{-1}], Δm_{SiO_2} is the residual mass of SiO_2 from TGA measurement [%], Δm_N is the mass of nitrogen from EA [%], M_N is the molar mass of nitrogen [g mol^{-1}], and N is the number of nitrogen atoms per functional group.

By taking into account the surface area per gram of silica, the number of functional groups per surface area $N_{FG\text{-}A}$ can be calculated according to eq 2:

$$N_{FG\text{-}A} = c_{FA} \times N_A \times \frac{1}{A} \times 10^{-18} \quad (2)$$

where $N_{FG\text{-}A}$ is the number of functional groups per area [nm^{-2}], n_{FG} is the molar concentration of functional groups per gram [mol g^{-1}], N_A is Avogadro's number, and A is the specific surface area of the nanoparticles per gram [m^2 g^{-1}].

Transmission electron microscopy (TEM) images were recorded on a JEOL JEM-2010 microscope. The samples were attached to Plano S160-3 copper grids by dispersing them in ethanol using an ultrasound cleaning bath, adding one drop (30 μL) on the copper grid and evaporating the solvent.

Dynamic light scattering (DLS) measurements were carried out by noninvasive backscattering on an ALV/CGS-3 compact goniometer system with an ALV/LSE-5003 correlator and multiple tau correlator at a wavelength of 632.8 nm (He−Ne Laser) and at a 90° goniometer angle. The dispersing media were purified before use with a syringe filter (200 nm mesh). The determination of the particle radius was carried out by the analysis of the correlation function via the g2(t) method followed by a linearized number-weighting (n.w.) of the distribution function.

Nitrogen sorption measurements were performed on a Sorptomatic 1900 instrument from Fisons Instruments at 77 K. The samples were degassed under vacuum at 60 °C for at least 2 h prior to measurement. The surface area was calculated according to Brunauer, Emmett, and Teller (BET).

Materials. Tetraethyl orthosilicate (TEOS) was provided by Wacker Silicones. 3-Aminopropyltriethoxysilane (APTES), 3-isocyanatopropyltriethoxysilane, 1,1′-(methylenedi-4,1-phenylene)-bismaleimide, isobutyl methyl ketone, dry toluene, dry dichloromethane, furan, dimethylfuran, hexamethyldisilazane, and dibutyltin dilaurate (95%) were purchased from Sigma-Aldrich and were used as received. All other solvents and chemicals were purchased from the central chemical depot of the Saarland University and dried according to standard procedures if necessary. Zinc chloride was purified in boiling dioxane with zinc dust and recrystallized from dioxane.

Synthesis of Silica Nanoparticles. The silica nanoparticles were synthesized according to a modified literature procedure.[20] In a 250 mL round-bottom flask, methanol (100 mL) was mixed with 51 mg (1.0 mmol) of 33% ammonia and 1.98 g (110 mmol) of water and stirred for 10 min. Then 10.41 g (50 mmol) of TEOS were added. The solution was stirred for 2 days, and a part of the particles was isolated to characterize the unmodified sample. The particles were precipitated with 100 mL of hexane and 50 mL of diethyl ether. Afterwards they were isolated and washed three times with ethanol by centrifugation at 13000 rpm and dried overnight in a vacuum oven (≈50 mbar) at 60 °C. Yield: 1.5 g silica particles; TEM: diameter 3.8 ± 0.9 nm; DLS: diameter 4.8 ± 0.8 nm; surface area: BET 750 m^2 g^{-1}.[12]

Synthesis of *N*-((3-Triethoxysilyl)propyl)maleimide 1. The synthesis was carried out following a literature procedure.[15] The reaction was carried out under argon atmosphere. In a 250 mL three-neck round-bottom flask equipped with a dropping funnel, 1.73 g (17.6 mmol) of maleic anhydride were dissolved in 60 mL of dry dichloromethane. A mixture of 3.90 g (17.6 mmol) of 3-(aminopropyl)triethoxysilane (APTES) and 20 mL of dry dichloromethane were added through a dropping funnel while stirring. After allowing the mixture to stand for 1 h at room temperature, the solvent was removed under vacuum. The intermediate product was collected as a white powder. ^1H NMR (200.13 MHz, $CDCl_3$, 25 °C) δ = 0.68 (t, ^3J = 7.7 Hz, 2H), 1.23 (t, ^3J = 7.0 Hz, 9H), 1.74 (p, ^3J = 7.7 Hz, 2H), 3.39 (q, ^3J = 6.5 Hz, 2H), 3.84 (q, ^3J = 7.0 Hz, 6H), 6.33 (s, 2H), 7.83 (br s, 1H). ^{13}C NMR (50.32 MHz, DMSO-d_6, 25 °C) δ = 7.80 (CH_2Si), 18.24 (CH_3CH_2O), 21.95 ($CH_2CH_2CH_2$), 42.64 (CH_2NH), 58.59 (CH_3CH_2O), 131.54 (=CHCONH), 136.08 (=CHCOOH), 165.56 (COOH), 166.03 (CONH).

In the next step, the intermediate product was dissolved in 60 mL of dry toluene, and 2.40 g (17.6 mmol) of zinc chloride were added at once. After the reaction mixture was heated to 80 °C, a solution of 2.84 g (17.6 mmol) of hexamethyldisilazane with 20 mL of toluene was added dropwise. The temperature was held during 5 h at 80 °C. After cooling, the solution was filtered to remove zinc chloride and the solvent was removed in vacuum. Yield: 5.12 g (17.0 mmol; 96.5%) of a colorless oily liquid. ^1H NMR (200.13 MHz, $CDCl_3$, 25 °C) δ = 0.55−0.64 (m, 2H), 1.22 (t, ^3J = 6.9 Hz, 9H), 1.62−1.78 (m, 2H), 3.51 (t, ^3J = 7.37 Hz, 2H), 3.81 (q, ^3J = 6.9 Hz, 6H), 6.68 (s, 2H). ^{13}C NMR (50.32 MHz, $CDCl_3$, 25 °C) δ = 7.49 (CH_2Si), 18.25 (CH_3CH_2O), 25.06 ($CH_2CH_2CH_2$), 45.36 (CH_2N), 58.44 (CH_3CH_2O), 134.21 (HC=CH), 171.10 (C=O). ^{29}Si NMR (59.63 MHz, $CDCl_3$, 25 °C) δ = −46.34. IR (cm^{-1}): 3099, 2974, 2932, 2887, 1770, 1703, 1440,

dx.doi.org/10.1021/cm303049k | Chem. Mater. XXXX, XXX, XXX−XXX

1406, 1365, 1255, 1220, 1166, 1101, 1072, 956, 829, 783, 756, 694, 453.

Synthesis of Protected Maleic Anhydride 3,6-Epoxy-1,2,3,6-tetrahydrophthalic Anhydride 4. The synthesis was carried out following a modified literature procedure.[16] In a 250 mL three-neck round-bottom flask under argon atmosphere, 20 g (0.204 mol) of the maleic anhydride and 14.04 g (0.206 mol) of furan were dissolved in 100 mL of toluene. The mixture was stirred for 24 h at room temperature. A white precipitate formed during this time. The solid was collected by filtration and washed two times with cold diethyl ether. The filtrate was reduced by rotary evaporation to 20 mL and cooled to 4 °C overnight. A second crop crystallized which was again collected by filtration and washed with diethyl ether. Finally, the crystals were dried in vacuum (≈10^{-2} mbar) overnight. Yield: 27.36 g (0.165 mol; 80.6%) of a white solid. ^{1}H NMR (200.13 MHz, $CDCl_3$, 25 °C) δ = 3.01 (s, 2 H), 5.40 (s, 2 H), 6.57 (s, 2 H). ^{13}C NMR (50.32 MHz, $CDCl_3$, 25 °C) δ = 47.52 (CH), 81.40 (CHO), 136.67 (C═C), 175.29 (C═O). IR (cm^{-1}): 3606, 3143, 3099, 3089, 3066, 3033, 3000, 2991, 1857, 1780, 1309, 1282, 1230, 1211, 1193, 1145, 1083, 1018, 948, 921, 902, 877, 848, 821, 800, 732, 690, 674, 634, 574, 428. Onset of decomposition (DSC, N_2, 15 K min^{-1}): 117.9 °C. Elemental analysis (%): Calcd for $C_8H_6O_4$: C 57.84, H 3.64, N 0.00; Found: C 56.75, H 3.71, N 0.00.

Synthesis of Protected 2-Hydroxyethylmaleimide 5. The synthesis was carried out following a modified literature procedure.[16] In a 100 mL round-bottom flask equipped with a reflux condenser, 5.80 g (35 mmol) of **4** were dissolved in 30 mL of dry MeOH. Afterwards 2.14 g (35 mmol) of ethanolamine were added dropwise at 0 °C. The mixture was refluxed for 24 h. The MeOH was removed by rotary evaporation, and the crude product was recrystallized from diethyl ether at −20 °C. The crystals were collected by filtration and washed with cold diethyl ether. Reducing the filtrate and recrystallizing again gained a second crop. The final product was dried in vacuum (≈10^{-2} mbar) overnight. Yield: 5.75 g (18.5 mmol; 52.7%) of a white solid. ^{1}H NMR (200.13 MHz, $CDCl_3$, 25 °C) δ = 0.86 (bs, 1H), 2.90 (s, 2H), 3.76 (m, 4H), 5.30 (s, 2H), 6.54 (s, 2H). ^{13}C NMR (50.32 MHz, $CDCl_3$, 25 °C) δ = 41.74 (CHOCHC═O), 47.46 (NCH_2), 60.22 (CH_2OH), 80.95 (HCO), 136.49 (C═C), 176.74 (C═O). IR (cm^{-1}): 3473, 3097, 3026, 3006, 2993, 2972, 2931, 2895, 1766, 1681, 1469, 1434, 1404, 1386, 1334, 1317, 1286, 1267, 1218, 1168, 1155, 1099, 1053, 1033, 1012, 958, 937, 916, 873, 850, 806, 771, 721, 703, 653, 594, 563, 530, 487, 428. Onset of decomposition (DSC, N_2, 15 K min^{-1}): 138.1 °C. Elemental analysis (%): Calcd for $C_{10}H_{11}NO_4$: C 57.41, H 5.30, N 6.70; Found: C 57.39, H 5.43, N 6.59.

Synthesis of Protected 2-(2,5-Dioxo-2,5-dihydro-1*H*-pyrrol-1-yl)ethyl 3-(Triethoxysilyl)propylcarbamate 2. The reaction was carried out under argon atmosphere. In a 100 mL three-neck round-bottom flask, 935 mg (3 mmol) of protected hydroxyethyl maleimide **5** was suspended in 10 mL of dry acetone. 890 mg (3.6 mmol) 3-Isocyanotopropyltriethoxysilane were added via a syringe while stirring. The solution was stirred at reflux overnight followed by the addition of 3 drops of dibutyltin dilaurate catalyst. The reaction mixture was refluxed for an additional 1 h. The crude mixture was concentrated under vacuum and washed with hexane three times. ^{1}H NMR (200.13 MHz, $CDCl_3$, 25 °C) δ = 0.56 (t, ^3J = 7.9 Hz, 2H), 1.17 (t, ^3J = 7.0 Hz, 9H), 1.54 (m, 2H), 2.84 (s, 2H), 3.09 (m, 2H), 3.67 (m, 2H), 3.77 (q, ^3J = 7.0 Hz, 6H), 4.13 (t, ^3J = 5.0 Hz, 2H), 5.20 (s, 2H), 6.48 (s, 2H). ^{13}C NMR (50.32 MHz, $CDCl_3$) δ 7.46 (CH_2Si), 18.24 (CH_3CH_2O), 23.17 ($CH_2CH_2CH_2$), 37.38 (OCH_2CH_2N), 41.74 (CHOCHC═O), 43.39 (CH_2NCO), 58.41 (CH_3CH_2O), 61.71 (CH_2OCN), 80.90 (HCO), 136.17 (C═C), 155.97 (NCOO), 170.48 (C═O). ^{29}Si NMR (59.63 MHz, $CDCl_2$, 25 °C) δ = −45.72. IR (cm^{-1}): 3356, 3080, 2974, 2927, 2885, 1774, 1701, 1600, 1512, 1436, 1388, 1361, 1336, 1240, 1222, 1190, 1166, 1099, 1074, 1022, 954, 877, 854, 771, 717, 648, 594, 530, 470, 428.

Syntheses of 1-(4-{[4-(2,5-Dioxo-3-{[3-(triethoxysilyl)-propyl]amino}pyrrolidin-1-yl)phenyl]methyl}phenyl)-2,5-dihydro-1*H*-pyrrole-2,5-dione 3. The reaction was carried out under argon atmosphere. In a 100 mL round-bottom flask, 2 g (5.8 mmol) of 1,1′-(methylenedi-4,1-phenylene)bismaleimide were dissolved in 50 mL of chloroform. 1.1 g (5 mmol) APTES were added, and the mixture was stirred for 12 h at RT. The crude product was used without further purification. ^{1}H NMR (200.13 MHz, $CDCl_3$, 25 °C) δ = 0.69 (t, ^3J = 8.0 Hz, 2H), 1.24 (t, ^3J = 7.0 Hz, 9H), 1.72 (m, 2H), 2.72 (m, 2H), 3.03−3.42 (m, 2H), 3.84 (q, ^3J = 7.0 Hz, 6H), 3.99 (s, 1H), 4.05 (s, 2H), 6.86 (s, 2H), 7.29 (m, 8H). ^{13}C NMR (50.32 MHz, $CDCl_3$) δ = 7.62, 18.09, 23.91, 36.62, 40.95, 46.48, 53.58, 58.11, 126.31, 126.51, 129.27, 129.51, 134.02, 140.02, 140.81, 168.16, 175.19, 176.31. ^{29}Si NMR (59.63 MHz, $CDCl_2$, 25 °C) δ = −46.03. IR (cm^{-1}): 3346, 3039, 2974, 2931, 2885, 1776, 1703, 1670, 1512, 1438, 1382, 1307, 1168, 1101, 1074, 1020, 952, 856, 811, 773, 671, 605, 513, 466, 408.

Solvent Exchange. Methanol was exchanged with isobutyl methyl ketone (IBMK) by adding 20 mL of IBMK to 50 mL of the particle suspension. A first fraction of methanol and excess ammonia were removed by rotary evaporation to reach a volume of approximately 10 mL. Then a second volume of 10 mL of IBMK was added, and the suspension was again concentrated to approximately 10 mL. This procedure was repeated two times. Afterwards the suspension was diluted with 90 mL of fresh IBMK.

Surface Functionalization of Silica Particles in IBMK. In a 250 mL three-neck round-bottom flask with a reflux condenser, 2 g of **1**, 3 g of **2**, or 3 g of the crude **3** was added to the silica particle suspension in IBMK and heated to 115 °C for 24 h. Afterwards the suspension was cooled to room temperature, and half of the solvent was removed by rotary evaporation. The particles were isolated by centrifugation at 13000 rpm for 10 min. Afterwards they were washed three times with acetone and dried overnight in a vacuum oven (≈50 mbar) at 80 °C. The particles were stored in a desiccator over P_2O_5. Yield: 0.8 g of yellowish particles.

■ ASSOCIATED CONTENT

Ⓢ Supporting Information

Supplementary infrared spectra, TGA/FTIR data, and UV/Vis spectra. This material is available free of charge via the Internet at http://pubs.acs.org.

■ AUTHOR INFORMATION

Corresponding Author

*E-mail: kickelbick@mx.uni-saarland.de.

Notes

The authors declare no competing financial interest.

■ ACKNOWLEDGMENTS

This work is supported by the German Research Society (DFG) through the priority program "Design and Generic Principles of Self-healing Materials" SPP 1568 (http://www.spp1568.uni-jena.de/).

■ REFERENCES

(1) Feichtenschlager, B.; Lomoschitz, C. J.; Kickelbick, G. *J. Colloid Interface Sci.* **2011**, *360*, 15.

(2) Lomoschitz Christoph, J.; Feichtenschlager, B.; Moszner, N.; Puchberger, M.; Muller, K.; Abele, M.; Kickelbick, G. *Langmuir* **2011**, *27*, 3534.

(3) Delattre, L.; Dupuy, C.; Babonneau, F. *J. Sol-Gel Sci. Technol.* **1994**, *2*, 185.

(4) Chen, X.; Wudl, F.; Mal, A. K.; Shen, H.; Nutt, S. R. *Macromolecules* **2003**, 36.

(5) Gandini, A.; Coelho, D.; Silvestre, A. J. D. *Eur. Polym. J.* **2008**, *44*, 4029.

(6) Gousse, C.; Gandini, A.; Hodge, P. *Macromolecules* **1998**, *31*, 314.

(7) Liu, X.; Zhu, M.; Chen, S.; Yuan, M.; Guo, Y.; Song, Y.; Liu, H.; Li, Y. *Langmuir* **2008**, *24*, 11967.

(8) Tesoro, G. C.; Sastri, V. R. *Ind. Eng. Chem. Prod. Res. Dev.* **1986**, *25*, 444.

(9) Costanzo, P. J.; Beyer, F. L. *Chem. Mater.* **2007**, *19*, 6168.

(10) Vejayakumaran, P.; Rahman, I. A.; Sipaut, C. S.; Ismail, J.; Chee, C. K. *J. Colloid Interface Sci.* **2008**, *328*, 81.
(11) Stoeber, W.; Fink, A.; Bohn, E. *J. Colloid Interface Sci.* **1968**, *26*, 62.
(12) Brunauer, S.; Emmett, P. H.; Teller, E. *J. Am. Chem. Soc.* **1938**, 60.
(13) Sing, K. S. W.; Everett, D. H.; Haul, R. A. W.; Moscou, L.; Pierotti, R. A.; Rouquerol, J.; Siemieniewska, T. *Pure Appl. Chem.* **1985**, *57*, 603.
(14) Huang, C.; Tassone, T.; Woodberry, K.; Sunday, D.; Green, D. L. *Langmuir* **2009**, *25*, 13351.
(15) Proupin-Perez, M.; Cosstick, R.; Liz-Marzan, L. M.; Salgueirino-Maceira, V.; Brust, M. *Nucleosides Nucleotides Nucleic Acids* **2005**, *24*, 1075.
(16) Adachi, K.; Achimuthu, A. K.; Chujo, Y. *Macromolecules* **2004**, 37.
(17) Beganskiene. *Mater. Sci. (Medziagotyra)* **2004**, *10*, 287.
(18) Knofel, C.; Martin, C.; Hornebecq, V.; Llewellyn, P. L. *J. Phys. Chem. C* **2009**, *113*, 21726.
(19) Parker, S. F.; Mason, S. M.; Williams, K. P. J. *Spectrochim. Acta, Part A* **1990**, *46A*, 315.
(20) Kickelbick, G.; Holzinger, D.; Ivanovici, S. Organically Functionalized Silica Nanoparticles. In *Materials Syntheses*; Schubert, U., Hüsing, N., Laine, R., Eds.; Springer: Wien, 2008; pp 127−133.